

FABRICATION OF CELLULAR CORDIERITE PREFORMS VIA BINDER JETTING

Dean Snelling¹, Christopher Williams¹, Carlos Suchicital², Alan Druschitz²

¹Design, Research, and Education for Additive Manufacturing Systems Laboratory; Department of Mechanical Engineering

²Department of Materials Science and Engineering
Virginia Tech, Blacksburg, VA

REVIEWED

ABSTRACT

Metal Matrix Composites (MMCs) combine two dissimilar materials – a metal as the matrix and a ceramic as the charge or insert to provide unique properties, e.g. low density, high specific strength, high specific modulus, and wear resistance. The ceramic inserts in these composite materials are limited to ceramic fibers and open cell stochastic ceramic foams due to geometric constraints imposed by traditional manufacturing processes. The geometric design freedom offered by Additive Manufacturing (AM) could enable a designer to realize ceramic preforms with complex cellular geometries that are designed to achieve multiple functions (e.g., low mass and increased stiffness). The goal of this work is to explore the use of Binder Jetting as a means of fabricating cordierite parts of designed mesostructure for use as ceramic preforms for MMCs. In this paper, the authors describe their exploration of the appropriate printing process parameters and post-process sintering parameters that enable successful fabrication of complex cordierite artifacts. Measurements of bulk density, linear shrinkage, porosity, and x-ray diffraction are conducted on pre- and post-sintered printed cordierite structures.

1. Introduction

Metal matrix composites are defined as a metal matrix reinforced by a constituent material, usually a ceramic [1], to provide materials with improved properties including low density, high specific strength, high specific modulus, high thermal conductivity, and wear resistance [2]. The matrix of the composite supports and transmits loads distributed to the secondary material used as reinforcement [3]. Metal matrix composites (MMC) can be broken down into two different fabrication processes: 1) solid state processing and 2) liquid state processing. Solid state processing includes using powder metallurgy and diffusion bonding. Liquid-state processing involves infiltrating, dispersion, spraying, and in-situ fabrication [2]. Many of the applications where metal matrix composites could have a significant impact have not been adopted because of the high cost to performance ratio [4] associated with the ceramic insert (e.g., fibers) used to create the reinforcement. For the case of ceramic fibers, the preforms are manufactured by mixing the fibers by press forming or suction forming. The liquid is removed and the preform is dried [5]. Such manufacturing processes are complex and the resulting parts are not reliable and can have unwanted phases. Furthermore, open cell ceramics (ceramic foams) have been used for the formation of MMCs to decrease the cost associated with preforms made with ceramic fibers [4]. But like MMCs fabricated with ceramic fibers, cost and geometric limitations are imposed by the manufacturing process associated with machining the final parts.

To alleviate these limitations, the authors propose the use of Binder Jetting additive manufacturing technology (AM) to manufacture complex ceramic cellular preforms for the

creation of MMCs. Using AM to form the ceramic pre-sintered pieces for MMCs would enable a manufacturer the freedom in complexity to create unique composites designed for specific applications. Traditional techniques for forming ceramics (pressing, casting, plastically forming the ceramics into a green part, followed by sintering in a pressure-less or pressure-assisted cycle [6]) are unable to manufacture complex geometries such as ordered cellular geometries (repeating unit cells featuring voids ordered throughout the structure). Manufacturing ordered cellular preforms for MMCs via AM would provide multiple functionality to the resultant part including decreased mass while increasing strength and stiffness and would allow an engineer to produce intricate geometries for specific design purposes (as opposed to that found in stochastic ceramic fiber and open cell preform techniques).

1.1. Binder Jetting Process and Capabilities

Binder Jetting is an AM technology that creates artifacts through the deposition of binder into a powder bed of raw material (Figure 1). Once a layer has been printed, the powder feed piston raises, the build piston lowers, and a counter-rotating roller spreads a new layer of powder on top of the previous layer. The subsequent layer is then printed and is adhered to the previous layer by the jetted binder. Binder Jetting is a versatile method of printing powdered materials. Any powder material that can be synthesized, deposited, and bound with a jettable binder may be used [7] including plaster, sand, metal, and other ceramics [8–10]. When printing ceramic powder, the resultant green part is sintered (and the binder pyrolyzed) to realize the final ceramic artifact.

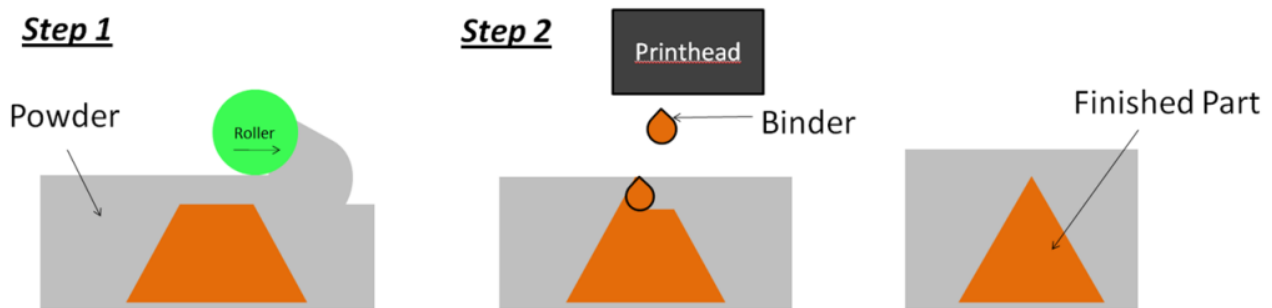


Figure 1. Binder Jetting AM Schematic

Other AM technologies such as powder bed fusion [11], vat photo polymerization [12], and extrusion [13] have been used to process ceramics, but they are outside the focus of this work. Binder Jetting is a focus of this work as it offers a low-cost and scalable means of producing ceramic artifacts with minimal constraints imposed on part topology. The technology is commercially offered by ExOne’s M-Print® and M-Flex® machines [14] and 3D Systems’ Professional ProJet® [15].

Ceramic parts have been successfully created via Binder Jetting to meet a variety of needs. Yoo and coauthors (1993) printed alumina powders to manufacture structural ceramic components that were 99.2% dense and had a flexural strength of 324 MPa [10]. Additionally, they were able to control the microstructure of zirconia toughened alumina (ZTA) by adding a stabilizer during the jetting process [16]. Seitz and coauthors’ (2005) used Binder Jetting to print hydroxyapatite (HA) ceramics to produce ceramic scaffolds for bone tissue engineering [17].

They were able to attain internal passage resolutions of 450 μm , wall thicknesses of 330 μm , and 22 MPa in compression. Sachs and coauthors (1990) tested the dimensional accuracy and part strength of printed parts from several ceramic powders including 320 grit (45 μm) aluminum oxide, silica, zirconia, zircon, and silicon carbide. Dimensional control was determined to be approximately ± 20 μm along 38 mm dimensions. Part strength was determined to be strong enough to handle and survive during pouring, but not strong enough to overcome the contraction of the metal during cooling. They determined that the geometric freedom offered by Binder Jetting could be used to efficiently prototype materials with specific application considerations and material properties [18].

Furthermore, AM of ceramics has been used to print preforms, but not specifically ordered cellular preforms. Sachs and coauthors (1990) explored the ability of Binder Jetting to create green ceramic preforms for infiltrating molten metal in order to manufacture metal matrix composites [18]. Additionally, they printed macroscopically toughened composites from SiC and Al 224 to eliminate cracks from propagating due to the interface [19]. Moon et al. (2001) printed carbon preforms with a designed mesostructure for reaction-infiltrating creating SiC-Si composites [20]. Unlike Sachs and coauthors, they utilized two materials to create a chemically bonded MMC. The print head speed was varied to obtain the desired preform microstructure and was controlled along the length of the complex preforms therefore controlling the carbon content along the part. This led to the ability to vary the reaction along the part and produce functionally graded SiC-C composites. The part contained three times the amount of binder saturation from one end to the other, resulting in a Si content of ~ 8 wt. % at the end with the highest binder saturation compared to ~ 24 wt. % at the end with the least binder. Unlike the work by Sachs and coauthors, and Moon et. al., this work uses precursor materials to generate cellular shapes for ceramic inserts.

1.2. Overview and Purpose of Work

The goal of this work is to form (print), sinter, and characterize ceramic cellular parts as precursors for MMCs. Specifically, an ExOne R2® system was used to fabricate cordierite ordered cellular structures. By using cellular geometries as MMC preforms, the authors strive to provide sufficient strength in bending and compression modes while decreasing the weight of the part [21]. A schematic of the manufacturing process is shown in Figure 2.

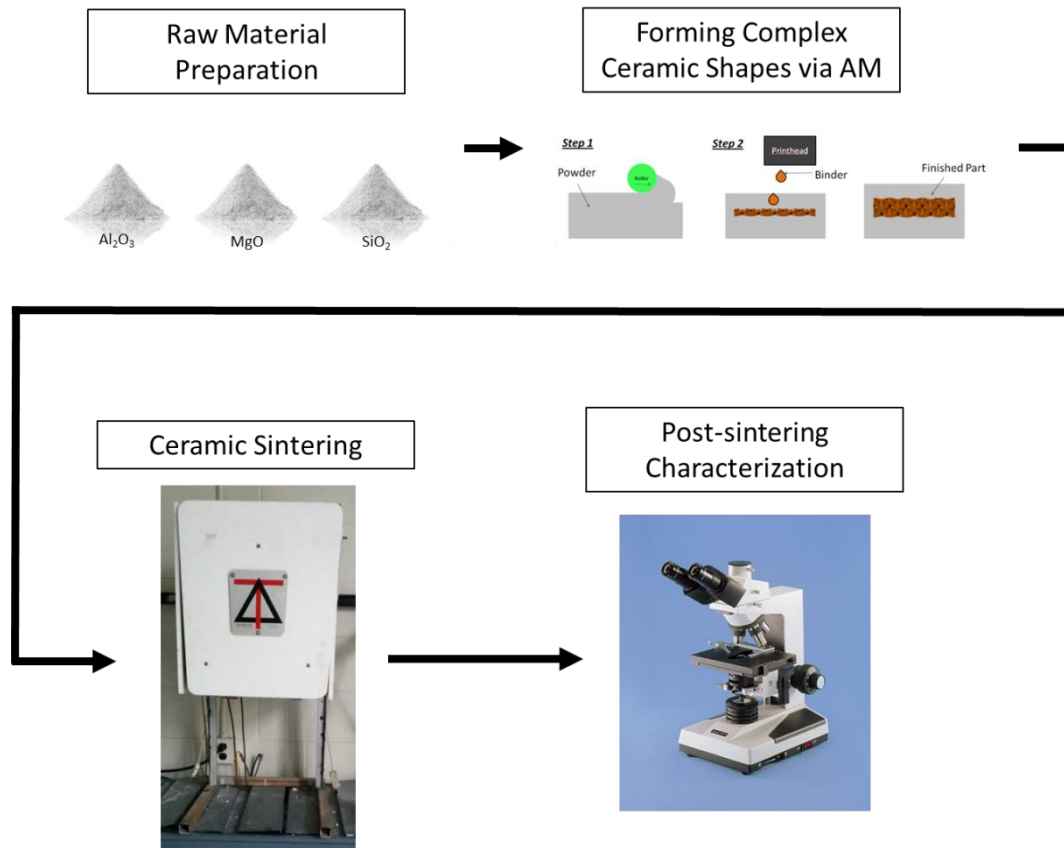


Figure 2. Proposed ceramic preform fabrication process

An overview of the materials and experimental methods employed in this study is presented in Section 2. The results from raw material characterization, printing parameters for the green part manufacture, sintering experimentation, and post-sintered characterization are given in Section 3. Closure is offered in Section 4 along with a discussion of future considerations.

2. Material Selection and Experimental Methods

2.1. Powder Selection

In order to manufacture suitable ceramic inserts for fabricating MMCs, the precursor materials were first selected. The materials were chosen based on the functional requirements of the manufacturing process (e.g., printing, sintering, and casting requirements). Several candidate materials were considered after successfully printing with the ExOne R2® system, yet, these did not meet the functional requirements of the manufacturing process. Since the MMCs are fabricated via metal casting, the final ceramic pieces were required to have high thermal shock resistance to eliminate the possibility of cracking during manufacture. Additionally, the parts needed to have lower sintering temperature to match the facility resources readily available at Virginia Tech.

Due to its poor thermal shock resistance behavior, Al_2O_3 alone was not considered a useful candidate for higher temperature cast metal matrix. However, when reacted with silica (SiO_2) and magnesia (MgO), the resultant material, cordierite ($2\text{MgO}\cdot 2\text{Al}_2\text{O}_3\cdot 5\text{SiO}_2$), can provide a

much improved thermal shock resistance. Cordierite was chosen because it has excellent thermal shock properties to withstand molten metal temperatures and also has a sintering temperature in the range of the electric furnace available [22]. In addition, the presence of a liquid phase can encourage higher final densities and decrease the required sintering temperature. Additionally, varying combinations of these materials would provide different properties for discrete applications and could be easily adjusted to fit further applications. For example, if increased strength is required and a sintering temperature is not a concern, the composition can be varied based on the properties of the resulting material. For these reasons cordierite was chosen as the candidate material.

2.2. Powder Preparation

Cordierite precursor materials were mixed using the amounts in Table 1 (derived from the molar composition given in Section 2.1). The raw materials were mixed in a container with Al₂O₃ pellets to ensure thorough blending and removal of agglomerates.

Table 1. Ceramic raw material mixtures

Ceramic	MgO (wt. %)	Al₂O₃ (wt. %)	SiO₂ (wt. %)
Cordierite (2MgO · 2 Al ₂ O ₃ · 5 SiO ₂)	13.78	34.86	51.36

The minimum mean particulate powder size for Binder Jetting is approximately 20 μm [23] and ideal shape for powder flow is spherical. However, off-the-shelf oxide powders for creating sintered ceramics are mostly angular containing smaller mean size distributions. Precursor powders typically are pressed and sintered to increase the final density with less shrinkage of the final part. A smaller mean particle size aids in reactivity, grain size, density requirements, rate of sintering, and temperature [24]. Printing ceramics via Binder Jetting is limited by the ability of the powder to be recoated by the binder evenly across the build tray. Dry powders with small particle sizes (<20 μm) are difficult to spread due to the cohesive strength of the high surface area of fine particles [10,23]. Additionally, spherical powders are desired for ease of spreading as opposed to angular particle shapes [19].

For this work, off-the-shelf ceramic powders were used as the raw materials for printing in the ExOne R2® system. To ensure their compatibility with the system, the particle size distribution of the precursor materials and the precursor mixture were analyzed using a Horiba LA-950® Laser Scattering Particle Size Distribution Analyzer and reported in Section 3.1.

2.3. Binder Jetting Printing Parameters

The goal of the proposed forming process was to manufacture geometrically intricate and accurate parts with sufficient green part strength for further handling, e.g., cleaning and sintering. During the forming process, printing parameters such as binder selection, layer thickness, heater temperature, binder saturation, spread speed, and drying rate were adjusted to achieve these objectives. These settings were determined by experimentally printing and examining green parts post-printing. For example, small rectangular parts were printed to ensure that the green parts had sufficient part strength to cure and be transferred to the furnace for sintering.

Additional octet truss unit cells (section A-B in Figure 3) were printed to determine the printing parameters of more complex shapes.

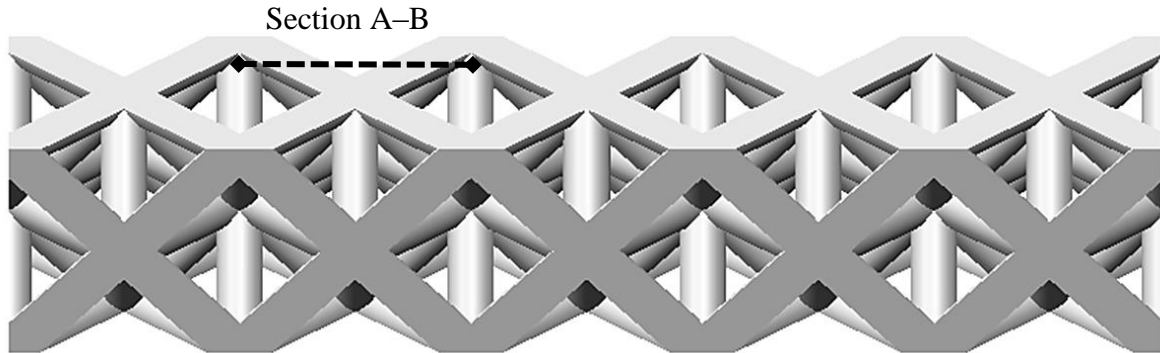


Figure 3. CAD Schematic of cellular repeating octet (A-B dotted line) truss pattern.

The printing parameters were adjusted to produce two distinct part types; i) solid parts for characterization purposes and ii) complex cellular parts for the purpose of creating metal-ceramic cellular structures (Section 3). It was determined by experimentally printing these two types of shapes that the binder saturation was different. Binder saturation was adjusted based on resultant green part strength. Excessive binder would decrease the quality of the final parts due to unwanted binder bleeding, while green parts with too little binder could have limited strength.

Furthermore, the drying rate produced by the overhead heater on the printer, was dependent on binder saturation values. The drying rate was the rate the overhead heater moves across the build tray after each layer is printed. The overhead heater on the AM system was used to dry binder after each layer to avoid excessive bleeding of binder by partially curing the binder.

The layer thickness was determined experimentally after printing the materials at different layer thicknesses. Any spreading defects during printing of thinner layers would produce potentially catastrophic results in the previous layer and therefore in the final part. In addition, the larger layer thickness provided much shorter overall build times. Because of the limitations of spreading fine angular powders (Section 3.1) thicker layers (200 μm) were tried and found to yield higher quality parts.

As previously noted, the binder used was ExOne's standard thermosetting binder that cures at 190°C. Once printing was completed, the green part was removed from the build bed, depowdered, and placed in an oven at the curing temperature for 2 hours. The cured binder gave strength to the part before placing in a high temperature environment for sintering.

2.4. Part Sintering

Small rectangular green parts that were used for testing printing parameters were also used for several firing trials to determine a satisfactory sintering temperature. Ceramic green specimens were placed in a furnace for firing with a 5°C/min ramp rate to the binder burnout temperature of 800°C for one hour, a 5°C/min ramp rate to the final sintering temperature with a dwell of one hour. Longer sintering cycles were tested and it was determined that change in temperature has a significantly larger effect on diffusion. The fired samples were removed from the furnace, at temperature (1350°C, 1360°C, 1375°C, and 1400°C) and at the end of the dwell period. The pieces were fired until parts acquired a glassy texture or appeared to be fully melted.

This observation determined a rudimentary range of temperatures for finding the preferred firing cycle. Relative bulk density and shrinkage characterization (Section 3.3.2) was performed on specimens sintered at that range of temperatures.

2.5. Ceramic Characterization

In addition to relative bulk density and shrinkage, the sintered ceramic parts were submitted to x-ray diffraction (XRD) and Optical Microscopy in order to determine the properties of the fired ceramic. The relative bulk density of the sintered ceramic parts was evaluated using the Archimedes Principle. Because the density determines the ultimate strength of the ceramic, this metric (along with shrinkage and porosity) was used to determine the sintering cycle. The parts were impregnated with oil before testing to seal the surface porosity and eliminate any water from penetrating interconnected porosity of the part (ASTM standard B962) [25].

The physical dimensions of the green parts were compared to those from the sintered part to obtain the apparent shrinkage. Additionally, the measurements from the CAD model were compared to those of the green and sintered parts to obtain the correct final part when modeling in CAD.

Optical microscopy was used to confirm the densification of the ceramic structure with each sintering cycle. Each printed ceramic block was mounted in an epoxy media and ground to 600 grit SiC paper, cleaned and examined. Optical micrographs of representative samples are shown in Section 3.2.

XRD analysis was completed on the final parts to determine how close the sintered ceramic sample's crystallographic structure came to the data found in the literature for a cordierite ceramic material. All samples to be examined were first ground to powder form with a mortar and pestle.

3. Results

3.1. Powder Characterization

The precursor powders were mixed and first tested with ExOne's standard binder (PM-B-SR2-05) used in the ExOne Binder Jetting AM equipment, to ensure that the material and the binder were compatible. The binder and precursor materials were mixed by hand, pressed into pellets, and sintered to verify that the parts, when printed, would retain their shape after sintering.

Following this verification of the binder/powder compatibility, the powder size distribution was analyzed to ensure that the powder could be successfully recoated during printing. The mean particle sizes of the precursor powders are shown in Table 2 and the number fraction (bar chart) and cumulative percent finer distributions (red line) of the mixed material are shown in Figure 4.

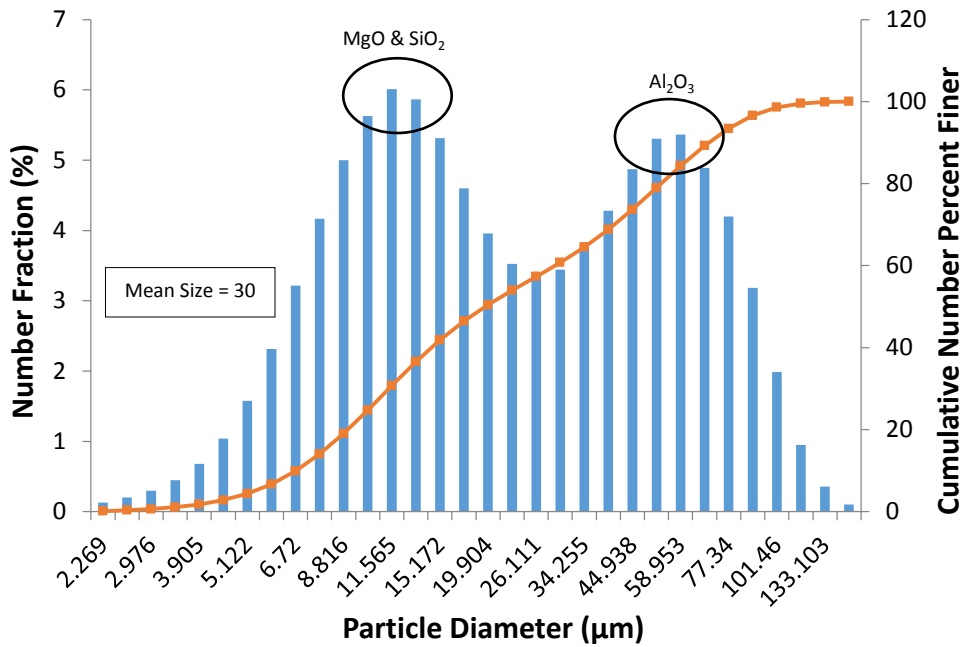


Figure 4. Particle size analysis: Number fraction and cumulative number percent finer distributions of cordierite precursor raw materials.

Table 2. Mean particle sizes of individual materials and cordierite precursor mixture

Material	Magnesia (MgO)	Alumina (Al ₂ O ₃)	Silica (SiO ₂)	Precursor Mixture
Mean Diameter (µm)	11.06	67.89	16.80	30.47

The cordierite precursor powder mixture had a mean particle size (30.5 µm), which is considered satisfactory for spreading in the AM system. However, not all individual materials were above the minimum size threshold (20 µm) (Table 2) and the trimodal distribution of particles in combination with the angular shape of the raw materials, resulted in a limited homogeneity of the powder mixture spreading step. In order to overcome the spreading restrictions of the available raw material, adjustments were made to the printing parameters in an attempt to maintain a consistent spread by the roller from the feed to the build tray of the AM system, as discussed in Section 3.2.

3.2. Experimental Printing Parameter Characterization

The printing parameters used for successful forming of a green part with sufficient strength are listed in Table 3.

Table 3. Printing parameters for printing cordierite precursor powders with ExOne R2® system

Parameter	Value	
Binder Selection	PM-B-SR2-05	
Layer Thickness	200 μm	
Heater Temperature	120-170°C	
Spread Speed	1 mm/s	
	Solid	Complex
Binder Saturation	150-190%	250%
Overhead Heater Travel Speed	1 mm/s	20 mm/s

Saturation values for complex parts required a higher amount of binder (250% of initial packing density) whereas solid objects required lower values (150-190% of initial packing density). High binder saturation values were not appropriate for solid objects, due to binder bleeding, which would decrease dimensional accuracy by excess bound powder from the surrounding support powder. Binder saturation was based on a printer input parameter – initial packing density. The ExOne R2® system was limited to the amount of additional pressure provided by the recoater to create denser “as printed” parts. Typically, spherical powders were used for better spread ability (Section 2.1) and have similar tap and apparent densities. The tap density could be measured and input into the printer. Additionally, adjusting the particle size distributions (mono-sized particles, bimodal, ternary, quaternary etc.) could be used to increase the initial packing density of the printed material.

Heating the jetted binder gave the printed part strength during and after printing the part in its green (unfired) state. The larger the saturation values (and consequently more binder) required more heat for curing. Solid parts required slower drying rate for the large volume of material to be dried/cured while complex parts used an accelerated rate to avoid over-drying and delamination of layers during depowdering the green part.

As discussed previously, spreading was satisfactory and was minimally controlled by adjusting spread speed. Setting the spread speed to the slowest value of 1 mm/s provided the best spread of the precursor materials. A slow spread speed minimized agglomerates from being drug across the new layer and instead created a tumble motion from the wave of new powder. After experimentation, the powder was able to spread evenly at low spread roller speeds (Section 2.3) with minor tracks from the previous due to agglomerates forming from the small particles in the wave of powder forming the new layer.

3.3. Sintered Part Characterization

3.3.1. Relative bulk density measurements

Based on the raw materials utilized in the precursor powder mixture for the AM process, the resulting fired ceramic part was expected to show a cordierite or cordierite like nature. Ceramics were found to have a glassy surface at approximately 1400°C but was too weak at 1350°C, therefore a temperature range of 1350°C-1400°C for sintering trials as discussed in 2.4.

Figure 5 shows the relative bulk density measured at different sintering temperatures and is based on a theoretical density for cordierite (2.51 g/cc)[26]. As expected, the density increased significantly until reaching approximately 92% at 1375°C. At this temperature, the ceramic parts reached the final stage of sintering (~90% density) and any further increase in temperature would generate an excess of the bonding liquid phase (with lower viscosity) and the integrity of the part would be compromised by slumping or by a complete melting [6].

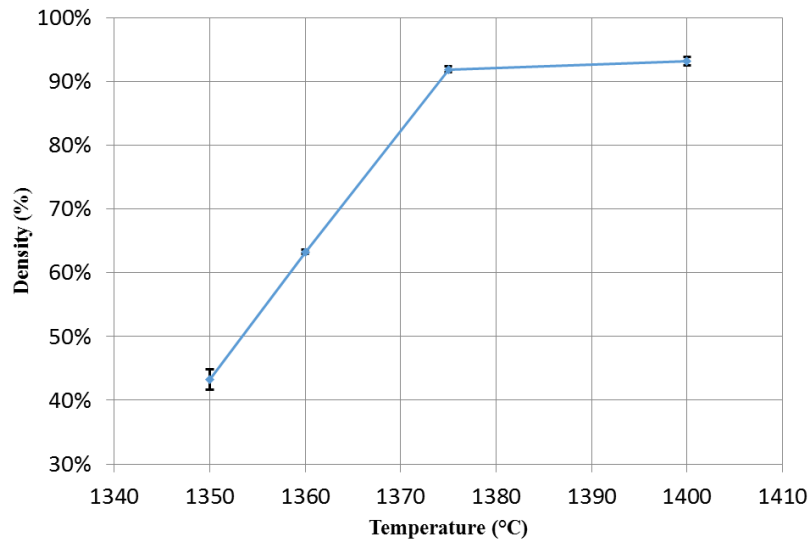


Figure 5. Relative bulk densities of fired ceramic parts as a function of the firing temperature

3.3.2. Shrinkage measurements

The shrinkage for each dimension as a result of sintering is shown in Figure 6. It was expected, given the correlation with the bulk density, that the shrinkage would be significantly greater at higher sintering temperatures. But it was also noted that with large shrinkage values, the ceramic parts experienced significant warping for both solid and complex objects. In both cases, the parts had a larger shrinkage in the Z-direction as compared to the X and Y directions. This is due to the effects of gravity on the part during the sintering process and can be corrected to meet geometrical dimensions by compensating the green part.

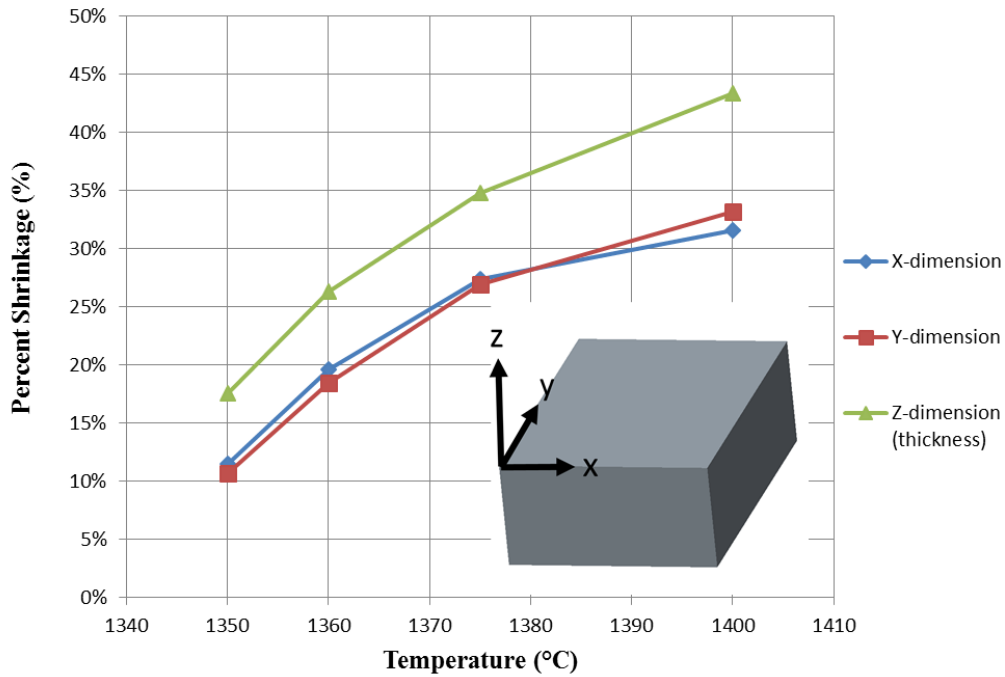


Figure 6. Ceramic shrinkage for ceramic parts at various sintering temperatures

3.3.3. *Optical microscopy of printed ceramics*

A macro sectioned piece and optical micrographs of representative ceramic samples are shown in Figure 7 and Figure 8. There was significant pore reduction in the samples fired from 1350°C to 1400°C in agreement with their relative bulk densities (Figure 5). Although the samples fired at 1400°C had the highest density, they also had the largest shrinkage and warping. Pores and ceramic material can be seen in Figure 7a and Figure 7b while micro cracks can be seen Figure 7c. As temperature increases, pores close as the diffusion increases in the ceramic. These samples presented a proliferation of micro cracks (~400 μm in length) in the bulk of the ceramic body, possibly due to a phase transformation of the ceramic materials at the higher temperature of 1400°C. Thus a firing temperature of 1375°C was selected as appropriate for the ceramic parts.

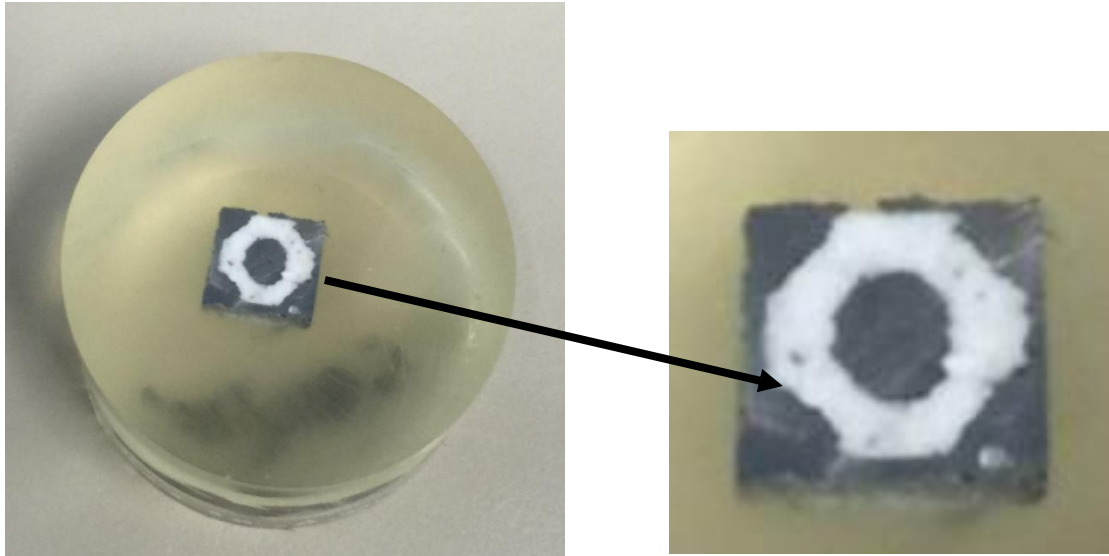


Figure 7. Sectioned ceramic microscopy piece.

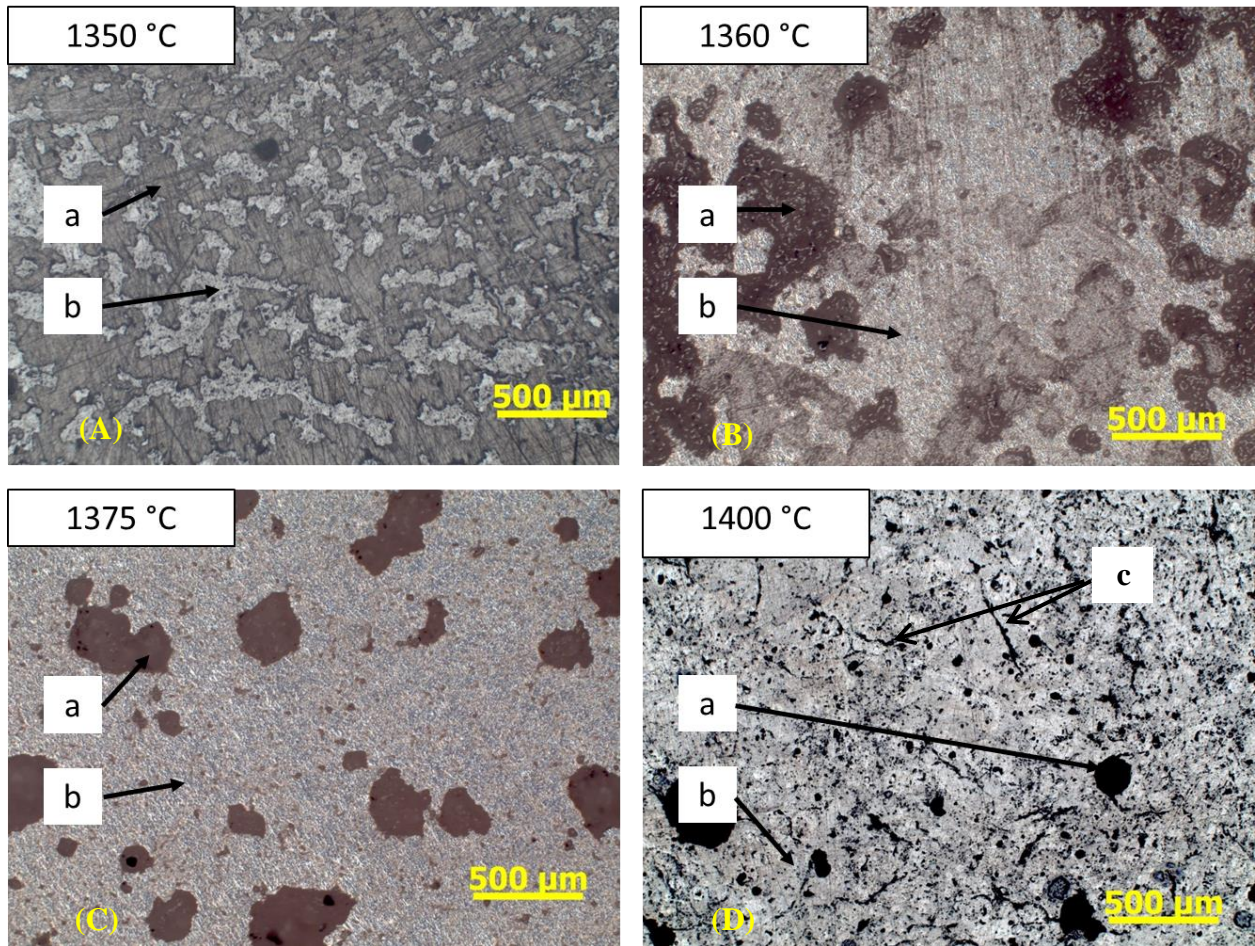


Figure 8. Optical microscopy (50x) of sintered ceramics at different sintering cycles: a) porosity with mounting media and b) ceramic material, c) micro cracks

3.3.4. X-Ray Diffraction (XRD) analysis

Both sets of the collected XRD data are shown in Figure 9. The figure shows the Bragg peaks used to compare the parts to the machine database to determine the printed and sintered raw material. The final sintering temperature chosen (1375°C) to fire the ceramic parts for the manufacture of MMCs correlated to a 78% match to the cordierite crystallographic structure found in the literature and was also the highest resulting match. The mismatch in matching the crystallographic structure of the AM built parts to that of cordierite may have been caused by the somewhat inhomogeneous spreading of the mixed raw materials required to make cordierite. Based on such 78% match, the true values of relative bulk density may differ slightly from those presented in Section 3.3.1 due to a change in theoretical density.

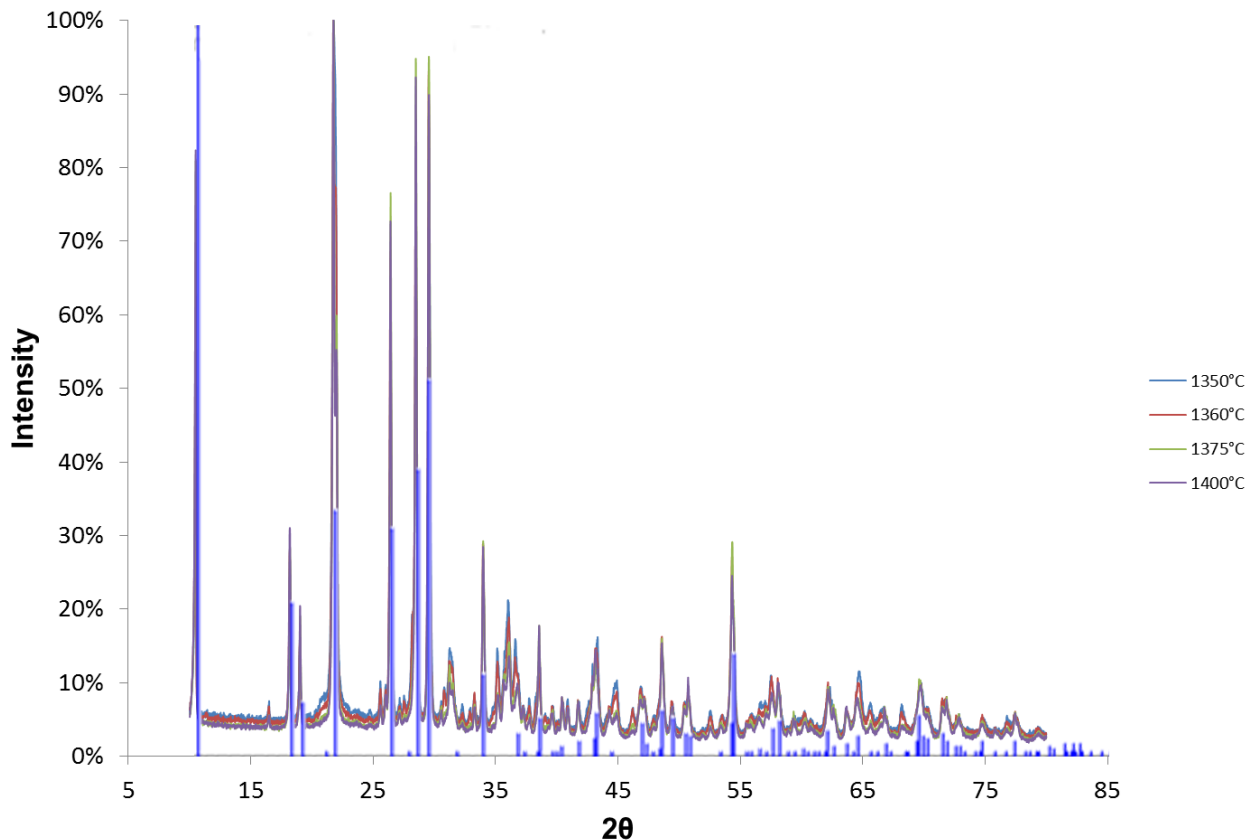


Figure 9. XRD data from different sintering temperatures of the ceramic samples and software values for cordierite

4. CONCLUSIONS AND FUTURE WORK

This work presented a novel process to manufacture complex ceramic geometries for the production of metal matrix composites. The overall research goal was to manufacture, test, and evaluate printed cordierite to withstand the environment of metal casting. The process included utilizing a ceramic fabricated by Additive Manufacturing from powder precursor materials, printing, sintering, and post sintering characterization.

Traditionally, manufacturers were bound to conventional forming techniques which geometrically limited the design. The use of AM technologies enables the user to manufacture complex ceramic parts that can be tailored for specific applications including MMCs. This work was focused on the use of AM to form the raw materials used for the production of a cordierite ceramic inserts for MMC production.

Additive manufacturing was used to print the precursor powders, alumina (Al_2O_3), silica (SiO_2), and magnesia (MgO), for the production of a cordierite ($2\text{MgO}\cdot 2\text{Al}_2\text{O}_3\cdot 5\text{SiO}_2$) like material. The correct print parameters (binder selection, layer thickness, heater temperature, binder saturation, spread speed, and drying rate) to successfully print the raw materials were determined experimentally. The materials were characterized pre-and-post sintering to evaluate the properties of the synthesized ceramic. It is recommended there is better control of the initial particle size (>20 micron mean diameter) and shape (from angular to spherical) to increase the flowability of the material during spreading, minimalizing agglomerates from forming and being drug across the build tray. Spherical particles will also provide more uniform initial packing density giving a consistent value for saturation settings.

In addition to using raw materials to produce cordierite inserts, the designer may also use printed materials with intricate geometries including those from other raw oxide materials (Al_2O_3 , mullite, enstatite, forsterite, sapphirine spinel, periclase, and corundum) to create ceramics for MMCs. However, the ceramic materials must be able to withstand the drastic thermal shock from the heat and the pressure of the metal matrix being casted.

5. ACKNOWLEDGEMENTS

The authors gratefully acknowledge Drs. Brian Lattimer and Patrick Summers of the ExtReMe Lab, the Department of Mechanical Engineering, and the Department of Materials Science and Engineering at Virginia Tech for their resources and support with equipment.

6. REFERENCES

- [1] Clyne, T. W., and Withers, P. J., 1993, *An Introduction to Metal Matrix Composites*, Cambridge University Press.
- [2] Suresh, S., Mortensen, A., and Needleman, A., 1993, *Fundamentals of Metal-Matrix Composites*, Butterworth-Heinemann, Boston.
- [3] Schleg, F. P., 2003, *Technology of Metalcasting*, American Foundry Society, Schaumburg, IL.
- [4] Standke, G., Müller, T., Neubrand, A., Weise, J., and Göpfert, M., 2010, “Cost-Efficient Metal-Ceramic Composites-Novel Foam-Preforms, Casting Processes and Characterisation,” *Adv. Eng. Mater.*, **12**(3), pp. 189–196.
- [5] Chawla, N., and Chawla, K. K., 2005, *Metal Matrix Composites*, Springer Science+Business Media.
- [6] Rahaman, M. N., 2003, *Ceramic Processing and Sintering*, Marcel Dekker, Inc.
- [7] Utela, B., Storti, D., Anderson, R., and Ganter, M., 2008, “A review of process development steps for new material systems in three dimensional printing (3DP),” *J. Manuf. Process.*, **10**(2), pp. 96–104.
- [8] Snelling, D. A., Kay, R., Druschitz, A., and Williams, C. B., 2012, “Mitigating Gas Defects in Castings Produced from 3D Printed Molds,” 117th Metalcasting Congress.
- [9] Gibson, I., Rosen, D. W., and Stucker, B., 2010, *Additive Manufacturing Technologies*.
- [10] Yoo, J., Cima, M. J., Khanuja, S., and Sachs, E. M., 1993, “Structural Ceramic Components by 3D Printing,” *International Solid Freeform Fabrication Symposium*, Austin, TX, pp. 40–50.
- [11] Lakshminarayan, U., Ogrydziak, S., and Marcus, H. L., 1990, “Selective Laser Sintering of Ceramic Materials,” *International Solid Freeform Fabrication Symposium*, Austin, TX, pp. 16–26.
- [12] Griffith, M. L., and Halloran, J. W., 1996, “Freeform Fabrication of Ceramics via Stereolithography,” *J. Am. Ceram. Soc.*, **79**(10), pp. 2601–2608.
- [13] Agarwala, M. K., Weeren, R. Van, Vaidyanathan, R., Langrana, N., Safari, A., Garofalini, S. H., and Danforth, S. C., 1990, “Structural Ceramics by Fused Deposition of Ceramics,” *International Solid Freeform Fabrication Symposium*, Austin, TX.
- [14] ExOne, “ExOne: Digital Part Materialization” [Online]. Available: <http://www.exone.com/materialization/what-is-digital-part-materialization/sand>.

- [15] 3D Systems, “Solutions: Metal Casting” [Online]. Available: <http://www.zcorp.com/en/Solutions/Castings-Patterns-Molds/spage.aspx>.
- [16] Yoo, J., Cima, M. J., and Suresh, S., 1995, “Fabrication and Microstructural Control of Advanced Ceramic Components by Three Dimensional Printing,” *Ceram. Eng. Sci. Proc.*, **16**(5), pp. 755–762.
- [17] Seitz, H., Rieder, W., Irsen, S., Leukers, B., and Tille, C., 2005, “Three-dimensional printing of porous ceramic scaffolds for bone tissue engineering,” *J. Biomed. Mater. Res. B. Appl. Biomater.*, **74**(2), pp. 782–8.
- [18] Sachs, E., Cima, M., Cornie, J., Brancazio, D., Brecht, J., Curodeau, A., Esterman, M., Fan, T., Harris, C., Kremmin, K., Lee, S. J., Pruitt, B., and Williams, P., 1990, “Dimensional Printing: Rapid Tooling and Prototypes Directly from CAD Representation,” *International Solid Freeform Fabrication Symposium*, Austin, TX, pp. 27–47.
- [19] Sachs, E., Cima, M., Cornie, J., Brancazio, D., Brecht, J., Curodeau, A., Fan, T., Khanuja, S., Lauder, A., Lee, J., and Michaels, S., 1993, “Three-Dimensional Printing: The Physics and Implications of Additive Manufacturing,” *CIRP Ann. - Manuf. Technol.*, **42**(1), pp. 257–260.
- [20] Moon, J., Caballero, A. C., Hozer, L., Chiang, Y.-M., and Cima, M. J., 2001, “Fabrication of functionally graded reaction infiltrated SiC–Si composite by three-dimensional printing (3DP™) process,” *Mater. Sci. Eng. A*, **298**(1-2), pp. 110–119.
- [21] Deshpande, V. S., Fleck, N. A., and Ashby, M. F., 2001, “Effective properties of the octet-truss lattice material,” *J. Mech. Phys. Solids*, **49**, pp. 1747–1769.
- [22] Boudchicha, M. R., Achour, S., and Harabi, A., 2001, “Crystallization and sintering of cordierite and anorthite based,” *J. Mater. Sci. Lett.*, **20**, pp. 215–217.
- [23] Cima, M. J., Haggerty, J. S., Sachs, E. M., and Williams, P. A., 1993, “Three-dimensional printing techniques.”
- [24] Sōmiya, S., Aldinger, F., Claussen, N., Spriggs, R. M., Uchino, K., Koumoto, K., and Kaneno, M., 2003, *Handbook of Advanced Ceramics*, Elsevier Inc.
- [25] ASTM Standard B962-14, 2014, “Standard Test Methods for Density of Compacted or Sintered Powder Metallurgy (PM) Products Using Archimedes’ Principle.”
- [26] Bedard, R. L., and Flanigen, E. M., 1990, “High Density Cordierite Ceramics from Zeolite.”